Site-specific electronic structure of imidazole and imidazolium in aqueous solutions

Journal:	*Physical Chemistry Chemical Physics*
Manuscript ID	CP-ART-11-2017-007885.R1
Article Type:	Paper
Date Submitted by the Author:	09-Feb-2018

Complete List of Authors:	Meyer, Frank; Julius-Maximilians-Universitat Wurzburg, Experimentelle Physik VII Blum, Monika; University of Nevada, Las Vegas, Department of Chemistry and Biochemistry Benkert, Andreas; Karlsruhe Institut of Technology, Insitute for Photon Science and Synchrotron Radiation Hauschild, Dirk; Karlsruhe Institute of Technology, Insitute for Photon Science and Synchrotron Radiation (IPS) Jeyachandran, Yekkoni Lakshmanan; Universität Heidelberg, Lehrstuhl für Angewandte Physikalische Chemie Wilks, Regan; Helmholtz-Zentrum Berlin für Materialien und Energie GmbH, Solar Energy Research Yang, Wanli; Lawrence Berkeley National Laboratory, Advanced Light Source Bär, Marcus; Helmholtz-Zentrum Berlin für Materialien und Energie GmbH, Renewable Energy Reinert, Friedrich; University of Würzburg, Experimental Physics 7 Heske , Clemens; University of Nevada, Las Vegas, Department of Chemistry and Biochemistry Zharnikov, Michael; University of Heidelberg, Institute of Physical Chemistry Weinhardt, Lothar; Karlsruhe Institut of Technology,

Site-specific electronic structure of imidazole and imidazolium in aqueous solutions

F. Meyer[1], M. Blum[2], A. Benkert[1,3], D. Hauschild[1,3,4], Y.L. Jeyachandran[5], R.G. Wilks[6], W. Yang[7], M. Bär[6], F. Reinert[1], C. Heske[2,3,4], M. Zharnikov[5], and L. Weinhardt[2,3,4*]

[1]*Universität Würzburg, Experimentelle Physik VII, Am Hubland, 97074 Würzburg, Germany*

[2] *Department of Chemistry and Biochemistry, University of Nevada, Las Vegas (UNLV), 4505 Maryland Parkway, NV 89154-4003, USA*

[3]*Institute for Photon Science and Synchrotron Radiation (IPS), Karlsruhe Institute of Technology (KIT), Hermann-v.-Helmholtz-Platz 1, 76344 Eggenstein-Leopoldshafen, Germany*

[4]*Institute for Chemical Technology and Polymer Chemistry (ITCP), Karlsruhe Institute of Technology (KIT), Engesserstr. 18/20, 76128 Karlsruhe, Germany*

[5]*Angewandte Physikalische Chemie, Universität Heidelberg, Im Neuenheimer Feld 253, 69120 Heidelberg, Germany*

[6]*Renewable Energy, Helmholtz-Zentrum Berlin für Materialien und Energie GmbH, Hahn-Meitner-Platz 1, 14109 Berlin, Germany*

[7]*Advanced Light Source (ALS), Lawrence Berkeley National Laboratory, 1 Cyclotron Road, Berkeley, CA 94720, USA*

*corresponding author: lothar.weinhardt@kit.edu

Abstract

The occupied and unoccupied electronic structure of imidazole ($C_3N_2H_4$) and imidazolium ($C_3N_2H_5^+$) in aqueous solutions is studied by x-ray emission spectroscopy (XES) and resonant inelastic soft x-ray scattering (RIXS). Both systems show distinct RIXS fingerprints with strong resonant effects. A comparison with calculated x-ray emission spectra of isolated imidazole and imidazolium suggests only a small influence of hydrogen bonding in the aqueous solution on the electronic structure of Im and ImH^+, and allows the attribution of specific spectral features to the non-equivalent nitrogen and carbon atoms in the molecules. In the case of nitrogen, this can also be achieved by site-selective resonant excitation. Furthermore, we find spectator shifts and symmetry selectivity in the RIXS spectra, as well as indications for rapid proton dynamics on the femtosecond timescale of the RIXS process, and derive the HOMO-LUMO gaps for the two molecules in aqueous solution.

Introduction

Imidazole ($C_3N_2H_4$, Im) is of high biological relevance, in particular as a building-block of the amino acid histidine, a subunit of the nucleobase purine, and many more. In addition to its biological relevance, imidazole also shows interesting proton transfer properties, which are utilized, in particular, to increase the performance of Nafion®-based proton exchange membranes (PEM) in fuel cells[1] and for the development of new anhydrous proton-conductive materials[2]. The protonated version of imidazole, imidazolium ($C_3N_2H_5^+$, ImH^+) represents an intermediate state during the proton transport and recently attracted particular interest in context of imidazolium-based ionic liquids, which create a complete new class of materials with a variety of unique and tunable properties[3].

In aqueous solution, a rapid (picosecond) exchange of protons between the two nitrogen atoms of Im was reported[4]. Due to this rapid exchange, the two nitrogen atoms of Im become indistinguishable for nuclear magnetic resonance spectroscopy (timescale of ~10^{-5} s)[5], while they can be clearly distinguished by

photoelectron spectroscopy (PES, timescale of ~10^{-17} s)[6], allowing the corresponding N 1s and C 1s core level positions in Im and ImH^+ to be measured[6]. Using PES, the occupied valence electronic structure has been investigated as well[7], but the spectrum is strongly dominated by solvent (i.e., water) contributions. Additional options are provided by other soft x-ray core level spectroscopies, namely x-ray absorption spectroscopy (XAS), x-ray emission spectroscopy (XES), and resonant inelastic soft x-ray scattering (RIXS), which promise atom- and, for non-equivalent atoms of the same kind, even site-specific information about the unoccupied (XAS, RIXS) and occupied (XES, RIXS) valence states, respectively. Recently, XAS has been used to study the self-association of Im at high concentrations in aqueous solution[8], comparing the XAS spectra of Im in gas and solid phase, as well as of aqueous Im solutions.

In this study, we use XES and RIXS to study both the occupied and unoccupied electronic structure of Im and ImH^+ in aqueous solution at high concentrations. As will be demonstrated below, this allows for an atom- and site-specific evaluation of the valence states and, additionally, gives us information about symmetry properties of the involved molecular orbitals and insights into ultra-fast proton dynamics.

Experimental Section

XES and RIXS experiments were performed at the roll-up port of beamline 8.0.1 at the Advanced Light Source (ALS), Lawrence Berkeley National Laboratory (Berkeley, USA), using the dedicated Solid And Liquid Spectroscopic Analysis (SALSA) experimental station[9]. This setup is equipped with a temperature-controlled flow-through liquid cell, in which the liquid is separated from ultra-high vacuum by a thin SiC (~150 nm, NTT) or Si_3N_4 (~100 nm, Silson) membrane and constantly refreshed with a frequency of ~700 Hz to avoid beam damage effects. The emitted x-ray spectra of the liquids are detected using a high-transmission soft x-ray spectrometer with a variable line space (VLS) grating[10]. For the present work, the combined resolving power $E/\Delta E$ (both x-ray spectrometer and beamline) was set to be better than 1000. The angle between the beamline and spectrometer was approx. 42º in the polarization plane of the undulator. Excitation and emission energy scales at the N and C K edges were calibrated using the

absorption spectra of N_2 gas[11] and HOPG[12], and the elastically scattered (Rayleigh) lines at these energies, respectively, leading to an uncertainty of the absolute energy scale of about ±0.2 eV.

Im was purchased from Alfa Aesar (purity >98%) and used without further purification. Two approx. 5M aqueous Im solutions were prepared with pH-values well above the equilibrium pKs of 7.05 (Ref. [13]) and used for the N K (pH-value of 10.3) and C K (pH = 11.1) measurements, respectively. Furthermore, two approx. 2.8 M ImH^+ solutions were prepared by adding HCl to aqueous Im solutions, and used for the N K (pH = 1.8) and C K (pH = 0.3) measurements, respectively. Note that at these concentrations, x-ray diffraction[14] and molecular dynamics simulations[15] suggest that some of the Im molecules directly interact with other Im molecules forming stacks and/or chains in aqueous solution.

XES and XAS spectra of an isolated imidazole molecule and an isolated imidazolium ion were calculated using the StoBe-DeMon package[16]. For geometry optimization and single-point calculations, Becke and Perdew exchange and correlation functionals[17–19] were used. To describe the valence electrons, we employed a double-zeta basis[20] and effective core potentials (ECPs)[21] with a 321/311/1 basis set for hydrogen and carbon, respectively. For nitrogen, a triple-zeta basis[20] was used. The core-excited atoms were described using diffuse IGLO-III basis sets[22]. The transition probabilities were calculated by the half core-hole transition potential method for XAS[23] and based on the ground-state Kohn-Sham eigenstates for XES, respectively. The energies of the transitions were determined using a Δ(Kohn-Sham self-consistent field) approach that includes differential relativistic effects associated with the removal of one electron from the 1*s* orbital[23]. This procedure leads to a reasonably appropriate description of the absolute emission energies and, thus, only small additional shifts are necessary to align the calculated emission energies with the experimental spectra. These additional shifts are given in Table 1 (the labels of the different atoms used in Tab. 1 are defined in Fig. 1).

Results and Discussion

Non-resonant x-ray emission spectra

The non-resonant N K emission spectra of Im and ImH^+ are shown in Figure 1 a) and b), respectively. Thick black lines represent the experimental spectra, vertical bars the calculated positions and transition probabilities of specific XES features, and lines of corresponding colors the calculations after broadening with Gaussian profiles. The line shape of each individual transition is determined by its vibrational envelope, which depends on the strength of the vibronic coupling for this transition[24], together with experimental and lifetime broadening. This complex line shape was approximated by Gaussians; their width was varied from 1.0 eV for the peak with highest emission energy to 2.0 eV for the lowest energy peaks. A good agreement between the calculation and the experiment with distinct differences in the case of ImH^+ (see discussion below) is achieved, which allows us to use the calculation for the assignment of the individual spectral features. Furthermore, we note that the rather good agreement between calculated (gas phase) and experimental (solution) spectra also suggests at most a small influence of hydrogen bonding in the aqueous solution on the electronic structure of Im and ImH^+.

The spectrum of Im is comprised of the contributions of the two non-equivalent nitrogen atoms in the molecule, shown in red (N1) and blue (N3) in Figure 1 a). The spectrum of N1 is dominated by a peak at ~394.0 eV, which is attributed to final states with holes in the HOMO-1 and HOMO-2 levels. In contrast, no appreciable intensity is observed for the HOMO level due to the small wave function overlap of the HOMO orbital of Im with the N1 1s orbital. This is visible in Figure 2, where calculated isodensity surfaces of the three highest occupied and three lowest unoccupied molecular orbitals of Im and ImH^+ are shown for a selected isosurface value (see Figure S1 in the Supplementary Information for the data obtained with another isosurface value). Here, we find the HOMO orbital to be located almost exclusively around the carbon atoms.

Towards lower emission energies, two additional spectral features at ~390.1 eV and ~385.8 eV, each consisting of several transitions, are observed in the N1 spectrum. Similar to the N1 spectrum, the N3 spectrum consists of three main spectral features. We find that transitions with the same final state appear at 2.0 eV higher emission energy for N3 than for N1, which is predominantly attributed to the higher binding energy of the 1s orbital of N3 compared to N1. The respective binding energy shift (~1.7 eV) was directly observed in the photoelectron spectra of aqueous Im[6]. The difference between these values is attributed to the difference in the involved states (e.g., a core hole in the photoemission final state, interacting with the outgoing electron, vs. a valence hole in the final state of XES). Furthermore, the emission intensities of some transitions with the same final state differ significantly for N1 and N3. In particular, in the case of N3, no intensity is observed for HOMO *and* HOMO-1, while, compared to N1, a higher emission intensity is observed at the low energy peak (at ~387.7 eV for N1). This is caused by the corresponding wave function overlap, as can exemplarily be seen in Figure 2: HOMO and HOMO-2 are quite symmetric with respect to N1 and N3, and thus the corresponding lines have similar intensities for both these atoms, while the HOMO-1 orbital only overlaps considerably with N1 and not N3.

For the protonated ImH^+, the molecule has a C_{2v} symmetry and the two nitrogen atoms N1 and N3 become equivalent, which leads to significant changes in the spectrum. The corresponding N1/N3 calculation (green in Fig. 1 b) broadly reproduces the main features of the experimental spectrum (thick black line). We assign the dominating peak at 395.3 eV to final states with a hole in the HOMO-1 orbital, while the small foot at ~397.1 eV is attributed to the HOMO orbital. The broad feature at 391.2 eV can be assigned to HOMO-2 through HOMO-4 with a prominent shoulder at ~390 eV, which we attribute to the HOMO-5 orbital. Finally, we find a well-separated emission feature at ~386.7 eV (HOMO-6 to HOMO-8) and some weak intensity around 382.5 eV (HOMO-9). At ~393.8 eV, the experimental spectrum shows a distinct feature, which is not reproduced by the calculation. Possible origins for this feature are the interaction of ImH^+ with the surrounding water molecules or ImH^+ ions and/or nuclear dynamics on the timescale of the x-ray emission process, both of which are not included in the calculation, while beam damage effects can be excluded due to the high flow rate in the liquid cell. For aqueous ammonia, we have in fact shown

previously that a weak spectral signature of hydrogen bonding orbitals, which are formed by a wave-function overlap with the neighboring water molecules, can be observed in-between the emission lines of the dissolved molecule[25]. However, similar to the case of aqueous ammonia, we expect the wave function overlap to be small. Hence, it appears more likely to assign the intensity at ~393.8 eV to nuclear dynamics (i.e., the removal of a proton on the timescale of the x-ray emission process). In a simple approximation, we "simulate" this effect by adding the calculated N1 spectrum of Im (called "N1*" in Figure 1 b) to the calculated ImH^+ spectrum. The theoretical spectra were weighted such that a reasonable agreement of the sum (shown with a black thin line) with the experimental spectrum is obtained. Similar ultra-fast proton dynamics on the timescale of the x-ray emission process have been observed for a number of small molecules, both in solution[25–35], as well as in gas phase[25,36–38]. Its occurrence highly depends on the potential energy surface in the excited state, which in turn can be influenced by the interaction with the surrounding molecules[25,27,28,31,39] (e.g., hydrogen bonding in a solution environment) or salt ions[40–42]. For the investigated ImH^+ solution, neighboring molecules of ImH^+ can be both water molecules as well as other ImH^+ ions. Following the approach in Ref. [43], the ratio n_{intact} between the spectral intensity of intact molecules and the total intensity, together with the N 1s core-hole life time τ of ~6.4 fs[44], can be used to give an estimate for the dissociation time $\tau_D = -\tau \cdot \ln(1 - n_{intact})$. We derive a value of ~13 fs.

Complementary to the N K measurements, the valence electronic structure at the location of the carbon atoms is probed by the C K emission spectra depicted in Figure 1 c) and d) for Im and ImH^+, respectively. Again, the calculated spectra were broadened with Gaussian profiles. Here, the widths were varied from 0.7 eV for Im (1.0 eV for Im^+) for the peak with highest emission energy to 1.3 eV for Im (2.0 eV for Im^+) for the lowest energy peaks for best spectral agreement. In contrast to the N K emission, strong intensity from transitions resulting in final states with a hole in the HOMO level can be observed in the C K emission spectrum of Im, caused by the strong overlap of the HOMO with the 1s orbitals of all carbon atoms. The calculated spectra of the three non-equivalent carbon atoms are shifted with respect to each other by 0.8 eV (C4 vs. C2) and 1.2 eV (C5 vs. C2), which correlates with the analogous shifts observed for the C 1s photoelectron spectra of aqueous Im[6]. In the experimental C K spectra, the HOMO levels give

rise to two emission lines at ~283.2 eV (C2) and ~282.1 eV (C4 and C5 combined). Furthermore, a weak line at 280.5 eV, an intense and broad feature around 276.9 eV, and another broad feature around 273.3 eV are found. In addition to these emission lines, a weak feature at ~286.0 eV is observed, which is not reproduced in the calculated spectrum. We tentatively attribute this feature to emission from a core-excitonic state[45].

Compared to the N atoms, the C atoms are much less affected by the protonation of the Im molecule. Consequently, the C K emission spectra of ImH^+ and Im show only small differences. In detail, we find a small shift of the HOMO → C 1s (C2) transition to lower emission energies, and the feature at ~280.5 eV in the spectrum of Im is less pronounced for ImH^+.

RIXS data

After the detailed assignment of the spectral features in the non-resonant emission spectra, the RIXS maps of Im and ImH^+ at the N K and C K edges will be discussed in the following. In these maps, presented in Figure 3, the intensity is color-coded as a function of emission and excitation energies. The maps can be divided into the participant and spectator regions. The participant region is located at higher emission energies, and the respective electronic final states correspond to the electronic ground state. The most prominent feature in this region is the Rayleigh line (i.e., the elastically scattered photons), which is visible as a diagonal line at equal excitation and emission energies. For excitation around the lower-lying absorption resonances (N K: at ~400.1 eV for Im and ~401.7 eV for ImH^+; C K: at ~286.9 eV for Im and ImH^+), a resonant increase in the Rayleigh line intensity is observed. This can be attributed to the formation of core-excitonic intermediate states, which enhances the probability for this specific decay channel[45]. At the same excitation energies, we find intensity extending from the elastic line to lower emission energies. This intensity can be attributed to emission with both, core-excitonic intermediate states, as well as vibronically-excited final states[46]. A closer look at all four maps reveals that the resonances of the Rayleigh line appear at slightly lower excitation energies than the inelastic tails of this

line, which can be explained by the interplay between wave packet dynamics in the intermediate state and the reduced duration time of the x-ray emission process for detuned excitation[27,46].

Below the absorption edge (Im and ImH^+) and at an excitation energy of ~403.2 eV (ImH^+), a loss feature is found in the N K RIXS maps that shifts parallel to the Rayleigh line. This is indicated by the dashed yellow line in Figure 3. Taking into account the vanishing transition probabilities for HOMO (Im and ImH^+) and HOMO-1 (Im), we attribute this loss feature to a HOMO-2 to LUMO transition for Im, and HOMO-1 to LUMO transition for ImH^+. This allows us to estimate the "optical“ HOMO-LUMO gap (i.e., including a valence exciton). For Im, the loss feature appears 7.0 eV below the Rayleigh line, which, together with the calculated separation between HOMO and HOMO-2 from Table S1, where the calculated orbital energies for Im and ImH^+ are presented, gives a HOMO-LUMO gap of 5.9 eV. This value is about 13% larger than our calculated gas phase HOMO-LUMO gap for Im (5.2 eV), and can also be compared to calculated values from literature (using a B3LYP functional) of 6.05 eV for gas phase and 6.53 eV for aqueous Im[47]. Note that a detailed study comparing the results of different functionals[48] found that the HOMO-LUMO gaps calculated with DFT using Becke and Perdew functionals, as in the present work, are usually close to the experimental value. In contrast, calculations using a B3LYP functional slightly overestimate this gap. We thus attribute the difference between our calculated and experimental values to the difference between Im in gas phase and aqueous solution. For ImH^+, the loss feature is found at 7.2 eV below the Rayleigh line. Together with the separation between HOMO and HOMO-1 from Table S1, we derive a value of 5.4 eV. This is slightly larger than our calculated value of 5.2 eV. Again, the difference might be attributed to the influence of the aqueous environment.

The spectator region, at emission energies below 397 eV (N K) and 284 eV (C K), corresponds to valence hole final states. Strong changes in peak positions and their relative and absolute intensities are observed upon variation of the excitation energy. For the detailed discussion of this region, we will also use the spectra presented in Figures 4 and 5. In Figure 4, partial fluorescence yield XAS spectra, derived from the maps in Figure 3 by integrating the emission intensity of the entire spectator region for each excitation

energy, are shown as thick black lines. Calculations are depicted below the experimental spectra using the same color code as in Figure 1. Calculations were broadened with Gaussians with full-width-of-half-maximum values of 0.8 eV (LUMO and LUMO+1 transitions) and 2.0 eV (all other transitions) for N K XAS and 0.6 eV (LUMO and LUMO+1 transitions) and 2.0 eV (all other transitions) for C K XAS.

Overall, a reasonable agreement between experiment and theory is achieved. The most prominent discrepancy occurs for the N K XAS spectrum of Im, where the calculation exhibits the LUMO+1 resonance in the N1 spectrum at 401.0 eV, whereas, in the experimental spectrum, no such peak is observed. This discrepancy can likely be attributed to the differences between Im in the gas phase (corresponding to isolated molecules as calculated) and in aqueous solution (experimental spectrum). In fact, the experimental electron energy loss spectrum (EELS) of gas-phase Im does exhibit a distinct peak around 401 eV[49] like in our calculation, while the experimental XAS spectrum of aqueous imidazole and the calculated spectrum of a small imidazole-water cluster do not exhibit this feature[8]. In fact, the influence of hydrogen bonding on the N K XAS spectra of a variety of small molecules in aqueous solution has been studied previously[8,25,35,50,51]. In particular, it was found that the hydrogen bonding environment can lead to energetic shifts of the peaks as well as to changes in relative emission intensities and an inhomogeneous broadening in the spectra. Based on these considerations and the comparison between experiment and calculations, the two resonances at 400.1 eV and 401.7 eV can be predominantly associated with transitions from the 1s levels of N1 and N3 to the LUMO, respectively. The weak feature at 403.3 eV can be assigned to the N3 1s → LUMO+1 transition. Note that the intensity of this feature is overestimated in the calculation, which again might be attributed to differences between gas and liquid phase. For ImH^+, both nitrogen atoms are protonated and thus the first peak in the XAS spectrum vanishes. This is reproduced by the gas-phase calculation and in accordance with both the experimental and calculated N K spectra of fully protonated histidine, which contains nitrogen atoms in very similar environments[35].

The C K spectra of both molecules are quite similar and are dominated by a broad peak at ~287 eV. For Im, this peak contains transitions from the 1s levels of all carbon atoms to the LUMO, while only C5 exhibits a strong matrix element for transitions to LUMO+1 (compare also the overlap between the calculated molecular orbitals in Figure 2 with the respective 1s orbitals). In the case of ImH^+, the main peak can be assigned to C2 1s → LUMO as well as C4/C5 1s → LUMO and LUMO+1 transitions.

The XAS spectra discussed above are reflected in the RIXS maps in Figure 3 as intensity variations in the excitation energy direction (i.e., vertical cuts). Taking *horizontal* cuts from the maps, we can now investigate the RIXS spectra at specific absorption resonances, which allows us to probe specific atomic sites and selected unoccupied molecular orbitals of the molecules. Figure 5 a) and b) shows N K RIXS spectra taken at selected excitation energies, which are also marked with white dashed lines in Figure 3, in comparison with the non-resonant spectra with an excitation energy of 424.0 eV (taken from Fig. 1).

The N K emission spectrum of Im with excitation at the first absorption resonance (400.1 eV, Figure 5 a, bottom) exhibits three main spectral features in the spectator region at 384.6, 390.1, and 393.1 eV, as well as the Rayleigh line at 400.1 eV. On the low emission-energy side of the Rayleigh line, a broad shoulder is observed that can be attributed to the excitation of vibrations in the final state. As discussed above, exclusively N1 is excited at the first absorption resonance. Taking this into account, the calculated N K emission spectrum for N1 (red) is shown for comparison after shifting it by 1.0 eV to lower emission energies with respect to non-resonant excitation, to account for the spectator shift[52]. It reproduces the experimental spectrum quite well, which suggests that in this case the spectral changes are mainly caused by the selective excitation of only this particular nitrogen site (N1). Similarly, the spectrum at the second absorption resonance (401.7 eV) strongly resembles the calculated spectrum for N3 only (shown in blue after shifting by 1.5 eV to lower emission energies), while as discussed above, the non-resonant spectrum is a superposition of the contributions from N1 and N3.

In the case of ImH^+, only the elastic line and no spectator emission is observed for excitation at 400.1 eV (Figure 5 b, bottom), in full agreement with the RIXS map (Figure 3 b). Comparing the spectrum excited

at 401.7 eV with the non-resonant one, we observe a shift of the main spectral features to lower emission energies, which can be attributed to spectator shifts. Furthermore, significant changes of the relative peak intensities are observed. While the center region of the spectrum (around 391.0 eV) becomes more prominent, we find reduced relative intensities of the features at approx. 396.0 eV and 393.9 eV. This can be attributed to symmetry selection[53] for excitation into the LUMO, reducing the intensity of emission involving the HOMO-1. In a simplified picture, which approximates the symmetry of the LUMO level by an *ungerade* symmetry and HOMO and HOMO-1 by a *gerade* symmetry, the corresponding transitions become forbidden. The fact that the corresponding emission line is still present and only reduced in intensity with respect to non-resonant excitation is likely due to the oversimplified nature of the gerade/ungerade approximation. Furthermore, nuclear dynamics will influence the symmetry restrictions, and, in case of ultrafast dissociation, might cause an additional redistribution of spectral weight.

Selected resonantly excited C K RIXS spectra of Im and ImH^+ are shown in Figures 5 c) and d), respectively, along with the reference non-resonant spectra taken at an excitation energy of 322.0 eV (also taken from Fig. 1). To improve the signal-to-noise ratio, the spectra for several excitation energies (ranges marked by A and B in Figures 3 c and d, resp.), were added up (within these ranges, no significant variations of the RIXS spectra were observed). For both Im and ImH^+, a strong resonance of the Rayleigh line occurs for excitation at A and B (note the multiplication factors of the participant energy region in Figs. 5 c and d). This indicates a strong interaction between the core hole and excited electron, i.e., the formation of a core exciton, which favors the elastic decay channel[45]. The intensity of the elastic line is strongest for excitation at A. For excitation at B, the core-excitonic state is still partly populated by the tails of the excitation giving rise to the spectral feature at ~286 eV, which is then also visible as a weak peak in the non-resonant spectra, as discussed above.

In the spectator region, strong spectator shifts of the emission lines can be found, which are marked for the two highest-energy peaks in Figures 5 c) and d). Furthermore, these two peaks are strongly reduced in intensity when exciting at A and B for both Im and ImH^+. In the case of ImH^+, the highest energy peak

nearly fully vanishes for excitation at B. The latter can be explained by the fact that at B, predominantly C4/C5 are excited (compare Figure 4 d), while the highest energy peak in the ImH^+ spectrum originates from emission involving C2. The overall reduction of the two HOMO-related high-energy peaks for both Im and ImH^+ is again attributed to symmetry selection for resonant excitation into the LUMO and LUMO+1 levels (approximately *ungerade*).

Conclusion

The electronic valence structure of Im and ImH^+ in aqueous solution has been studied using XES and RIXS at the N and C K edges. A detailed spectral interpretation is presented and supported by calculated spectra of the isolated molecules. By comparison with the calculated spectra, the spectral contributions of the non-equivalent nitrogen and carbon atoms, as well as of specific molecular orbitals, can be identified in the XES and XAS spectra. The rather good agreement between calculated and experimental spectra suggests only a small influence of the hydrogen bonding environment in the aqueous solution on the electronic structure of Im and ImH^+. In the case of ImH^+, we find evidence for nuclear dynamics on the timescale of the x-ray emission process, ultimately leading to an ultrafast dissociation of the molecule.

Upon resonant excitation, significant changes in both the N and C K spectra are observed. We find that, in the case of the N K emission of Im, the contributions of the two non-equivalent nitrogen atoms can be separated experimentally by excitation at the specific absorption resonances. Furthermore, we find spectator shifts in all resonant spectra (N and C K), as well as the suppression of HOMO and HOMO-1 related emissions caused by symmetry selection according to the symmetry of the LUMO state. Based on the presented RIXS maps, we derive values for the HOMO-LUMO gaps of both molecules in aqueous solution (5.9 eV for Im and 5.4 eV for ImH^+, respectively).

The results paint a detailed picture of the electronic structure of this important molecule and its solutions, and form the basis for the study of Im and ImH^+ in their various applications and as a building block of histidine or larger biologically relevant molecules.

Acknowledgement

This work was supported by the German Research Society (DFG; projects No. RE 1469/7-1 and ZH 63/16-1). This research used resources of the Advanced Light Source, which is a DOE Office of Science User Facility under contract no. DE-AC02-05CH11231. M. Bär and R.G. Wilks acknowledge funding by the Impuls- und Vernetzungsfonds of the Helmholtz Association (VH-NG423).

References

1 L. Yang, B. Tang and P. Wu, A novel proton exchange membrane prepared from imidazole metal complex and Nafion for low humidity, *J. Membr. Sci.*, 2014, **467**, 236–243.

2 S. Bureekaew, S. Horike, M. Higuchi, M. Mizuno, T. Kawamura, D. Tanaka, N. Yanai and S. Kitagawa, One-dimensional imidazole aggregate in aluminium porous coordination polymers with high proton conductivity, *Nat. Mater.*, 2009, **8**, 831–836.

3 M. D. Green and T. E. Long, Designing Imidazole-Based Ionic Liquids and Ionic Liquid Monomers for Emerging Technologies, *Polym. Rev.*, 2009, **49**, 291–314.

4 W. Münch, K.-D. Kreuer, W. Silvestri, J. Maier and G. Seifert, The diffusion mechanism of an excess proton in imidazole molecule chains: first results of an ab initio molecular dynamics study, *Solid State Ion.*, 2001, **145**, 437–443.

5 M. Munowitz, W. W. Bachovchin, J. Herzfeld, C. M. Dobson and R. G. Griffin, Acid-base and tautomeric equilibriums in the solid state: nitrogen-15 NMR spectroscopy of histidine and imidazole, *J. Am. Chem. Soc.*, 1982, **104**, 1192–1196.

6 D. Nolting, N. Ottosson, M. Faubel, I. Hertel and B. Winter, Pseudoequivalent nitrogen atoms in aqueous imidazole distinguished by chemical shifts in photoelectron spectroscopy, *J. Am. Chem. Soc.*, 2008, **130**, 8150.

7 B. Jagoda-Cwiklik, P. Slavíček, L. Cwiklik, D. Nolting, B. Winter and P. Jungwirth, Ionization of Imidazole in the Gas Phase, Microhydrated Environments, and in Aqueous Solution, *J. Phys. Chem. A*, 2008, **112**, 3499–3505.

8 M. J. Thomason, C. R. Seabourne, B. M. Sattelle, G. A. Hembury, J. S. Stevens, A. J. Scott, E. F. Aziz and S. L. M. Schroeder, Self-association of organic solutes in solution: a NEXAFS study of aqueous imidazole, *Faraday Discuss.*, 2015, **179**, 269–289.

9 M. Blum, L. Weinhardt, O. Fuchs, M. Bär, Y. Zhang, M. Weigand, S. Krause, S. Pookpanratana, T. Hofmann, W. Yang, J. D. Denlinger, E. Umbach and C. Heske, Solid and liquid spectroscopic analysis (SALSA) -a soft x-ray spectroscopy endstation with a novel flow-through liquid cell, *Rev. Sci. Instrum.*, 2009, **80**, 123102.

10 O. Fuchs, L. Weinhardt, M. Blum, M. Weigand, E. Umbach, M. Bär, C. Heske, J. Denlinger, Y. D. Chuang, W. McKinney, Z. Hussain, E. Gullikson, M. Jones, P. Batson, B. Nelles and R. Follath, High-resolution, high-transmission soft x-ray spectrometer for the study of biological samples, *Rev. Sci. Instrum.*, 2009, **80**, 63103.

11 M. Kato, Y. Morishita, M. Oura, H. Yamaoka, Y. Tamenori, K. Okada, T. Matsudo, T. Gejo, I. H. Suzuki and N. Saito, Absolute photoionization cross sections with ultra-high energy resolution for Ar, Kr, Xe and N2 in inner-shell ionization regions, *J. Electron Spectrosc. Relat. Phenom.*, 2007, **160**, 39–48.

12 B. Watts and H. Ade, A simple method for determining linear polarization and energy calibration of focused soft X-ray beams, *J. Electron Spectrosc. Relat. Phenom.*, 2008, **162**, 49–55.

13 D. R. Lide, *CRC Handbook of Chemistry and Physics, Internet Version 2005. Ed. by D. R. Lide. Boca Raton, FL: CRC Press, 2005*, .

14 L. Gontrani, R. Caminiti, L. Bencivenni and C. Sadun, Molecular aggregation phenomena in solution: an energy dispersive X-ray diffraction study of concentrated imidazole water solutions, *Chem. Phys. Lett.*, 1999, **301**, 131–137.

15 S. Y. Liem, M. S. Shaik and P. L. A. Popelier, Aqueous Imidazole Solutions: A Structural Perspective from Simulations with High-Rank Electrostatic Multipole Moments, *J. Phys. Chem. B*, 2011, **115**, 11389–11398.

16 *StoBe-deMon version 3.1 (2011), K. Hermann and L.G.M. Pettersson, M.E. Casida, C. Daul, A. Goursot, A. Koester, E. Proynov, A. St-Amant, and D.R. Salahub. Contributing authors: V. Carravetta, H. Duarte,*

C. Friedrich, N. Godbout, J. Guan, C. Jamorski, M. Leboeuf, M. Leetmaa, M. Nyberg, S. Patchkovskii, L. Pedocchi, F. Sim, L. Triguero, and A. Vela, .
17 A. D. Becke, Density-functional exchange-energy approximation with correct asymptotic behavior, *Phys. Rev. A*, 1988, **38**, 3098–3100.
18 J. P. Perdew, Density-functional approximation for the correlation energy of the inhomogeneous electron gas, *Phys. Rev. B*, 1986, **33**, 8822–8824.
19 J. P. Perdew, Erratum: Density-functional approximation for the correlation energy of the inhomogeneous electron gas, *Phys. Rev. B*, 1986, **34**, 7406–7406.
20 N. Godbout, D. R. Salahub, J. Andzelm and E. Wimmer, Optimization of Gaussian-type basis sets for local spin density functional calculations. Part I. Boron through neon, optimization technique and validation, *Can. J. Chem.*, 1992, **70**, 560–571.
21 L. G. M. Pettersson, U. Wahlgren and O. Gropen, Effective core potential parameters for first- and second-row atoms, *J. Chem. Phys.*, 1987, **86**, 2176–2184.
22 W. Kutzelnigg, U. Fleischer and M. Schindler, *The IGLO-Method: Ab-initio Calculation and Interpretation of NMR Chemical Shifts and Magnetic Susceptibilities". en. Deuterium and Shift Calculation. NMR Basic Principles and Progress*, Springer, Heidelberg, 1990.
23 L. Triguero, L. G. M. Pettersson and H. Ågren, Calculations of near-edge x-ray-absorption spectra of gas-phase and chemisorbed molecules by means of density-functional and transition-potential theory, *Phys. Rev. B*, 1998, **58**, 8097–8110.
24 F. Hennies, S. Polyutov, I. Minkov, A. Pietzsch, M. Nagasono, H. Ågren, L. Triguero, M.-N. Piancastelli, W. Wurth, F. Gel'mukhanov and A. Föhlisch, Dynamic interpretation of resonant x-ray Raman scattering: Ethylene and benzene, *Phys. Rev. At. Mol. Opt. Phys.*, 2007, **76**, 32505.
25 L. Weinhardt, E. Ertan, M. Iannuzzi, M. Weigand, O. Fuchs, M. Bär, M. Blum, J. D. Denlinger, W. Yang, E. Umbach, M. Odelius and C. Heske, Probing hydrogen bonding orbitals: resonant inelastic soft X-ray scattering of aqueous NH3, *Phys. Chem. Chem. Phys.*, 2015, **17**, 27145–27153.
26 M. Blum, M. Odelius, L. Weinhardt, S. Pookpanratana, M. Bär, Y. Zhang, O. Fuchs, W. Yang, E. Umbach and C. Heske, Ultrafast Proton Dynamics in Aqueous Amino Acid Solutions Studied by Resonant Inelastic Soft X-ray Scattering, *J. Phys. Chem. B*, 2012, **116**, 13757.
27 L. Weinhardt, M. Weigand, O. Fuchs, M. Bär, M. Blum, J. D. Denlinger, W. Yang, E. Umbach and C. Heske, Nuclear dynamics in the core-excited state of aqueous ammonia probed by resonant inelastic soft x-ray scattering, *Phys. Rev. B*, 2011, **84**, 104202.
28 L. Weinhardt, O. Fuchs, M. Blum, M. Bär, M. Weigand, J. D. Denlinger, Y. Zubavichus, M. Zharnikov, M. Grunze, C. Heske and E. Umbach, Resonant X-ray emission spectroscopy of liquid water: Novel instrumentation, high resolution, and the "map" approach, *J. Electron Spectrosc. Relat. Phenom.*, 2010, **177**, 206–211.
29 O. Fuchs, M. Zharnikov, L. Weinhardt, M. Blum, M. Weigand, Y. Zubavichus, M. Bär, F. Maier, J. D. Denlinger, C. Heske, M. Grunze and E. Umbach, Isotope and temperature effects in liquid water probed by x-ray absorption and resonant x-ray emission spectroscopy, *Phys. Rev. Lett.*, 2008, **100**, 27801.
30 M. Odelius, H. Ogasawara, D. Nordlund, O. Fuchs, L. Weinhardt, F. Maier, E. Umbach, C. Heske, Y. Zubavichus, M. Grunze, J. D. Denlinger, L. G. M. Pettersson and A. Nilsson, Ultrafast core-hole-induced dynamics in water probed by x-ray emission spectroscopy, *Phys. Rev. Lett.*, 2005, **94**, 227401.
31 S. Schreck, A. Pietzsch, K. Kunnus, B. Kennedy, W. Quevedo, P. S. Miedema, P. Wernet and A. Föhlisch, Dynamics of the OH group and the electronic structure of liquid alcohols, *Struct. Dyn.*, 2014, **1**, 54901.
32 A. Pietzsch, F. Hennies, P. S. Miedema, B. Kennedy, J. Schlappa, T. Schmitt, V. N. Strocov and A. Föhlisch, Snapshots of the Fluctuating Hydrogen Bond Network in Liquid Water on the Sub-Femtosecond Timescale with Vibrational Resonant Inelastic x-ray Scattering, *Phys. Rev. Lett.*, 2015, **114**, 88302.

33 T. Tokushima, Y. Harada, O. Takahashi, Y. Senba, H. Ohashi, L. G. M. Pettersson, A. Nilsson and S. Shin, High resolution X-ray emission spectroscopy of liquid water: The observation of two structural motifs, *Chem Phys Lett*, 2008, **460**, 387.
34 M. Odelius, Molecular dynamics simulations of fine structure in oxygen K -edge x-ray emission spectra of liquid water and ice, *Phys. Rev. B*, 2009, **79**, 144204.
35 S. Eckert, J. Niskanen, R. M. Jay, P. S. Miedema, M. Fondell, B. Kennedy, W. Quevedo, M. Iannuzzi and A. Föhlisch, Valence orbitals and local bond dynamics around N atoms of histidine under X-ray irradiation, *Phys. Chem. Chem. Phys.*, 2017, **19**, 32091–32098.
36 L. Weinhardt, A. Benkert, F. Meyer, M. Blum, R. G. Wilks, W. Yang, M. Bär, F. Reinert and C. Heske, Nuclear dynamics and spectator effects in resonant inelastic soft x-ray scattering of gas-phase water molecules, *J. Chem. Phys.*, 2012, **136**, 144311.
37 A. Benkert, F. Meyer, D. Hauschild, M. Blum, W. Yang, R. G. Wilks, M. Bär, F. Reinert, C. Heske and L. Weinhardt, Isotope Effects in the Resonant Inelastic Soft X-ray Scattering Maps of Gas-Phase Methanol, *J. Phys. Chem. A*, 2016, **120**, 2260–2267.
38 V. V. da Cruz, E. Ertan, R. C. Couto, S. Eckert, M. Fondell, M. Dantz, B. Kennedy, T. Schmitt, A. Pietzsch, F. F. Guimarães, H. Ågren, F. Gel'mukhanov, M. Odelius, A. Föhlisch and V. Kimberg, A study of the water molecule using frequency control over nuclear dynamics in resonant X-ray scattering, *Phys. Chem. Chem. Phys.*, 2017, **19**, 19573–19589.
39 K. M. Lange, M. Soldatov, R. Golnak, M. Gotz, N. Engel, R. Könnecke, J.-E. Rubensson and E. F. Aziz, X-ray emission from pure and dilute H_{2}O and D_{2}O in a liquid microjet: Hydrogen bonds and nuclear dynamics, *Phys. Rev. B*, 2012, **85**, 155104.
40 Y. L. Jeyachandran, F. Meyer, A. Benkert, M. Bär, M. Blum, W. Yang, F. Reinert, C. Heske, L. Weinhardt and M. Zharnikov, Investigation of the Ionic Hydration in Aqueous Salt Solutions by Soft X-ray Emission Spectroscopy, *J. Phys. Chem. B*, 2016, **120**, 7687–7695.
41 Y. L. Jeyachandran, F. Meyer, S. Nagarajan, A. Benkert, M. Bär, M. Blum, W. Yang, F. Reinert, C. Heske, L. Weinhardt and M. Zharnikov, Ion-Solvation-Induced Molecular Reorganization in Liquid Water Probed by Resonant Inelastic Soft X-ray Scattering, *J. Phys. Chem. Lett.*, 2014, **5**, 4143–4148.
42 Z. Yin, I. Rajkovic, S. Thekku Veedu, S. Deinert, D. Raiser, R. Jain, H. Fukuzawa, S. Wada, W. Quevedo, B. Kennedy, S. Schreck, A. Pietzsch, P. Wernet, K. Ueda, A. Föhlisch and S. Techert, Ionic Solutions Probed by Resonant Inelastic X-ray Scattering, *Z. Für Phys. Chem.*
43 A. Naves de Brito, A. Naves de Brito, O. Björneholm, J. S. Neto, A. B. Machado, S. Svensson, A. Ausmees, S. J. Osborne, L. J. Sæthre, H. Aksela, O.-P. Sairanen, A. Kivimäki, E. Nõmmiste and S. Aksela, Fast dissociation of resonantly core excited H2S studied by vibrational and temporal analysis of the Auger spectra, *J Mol Struct THEOCHEM*, 1997, **394**, 135.
44 K. C. Prince, M. Vondráček, J. Karvonen, M. Coreno, R. Camilloni, L. Avaldi and M. de Simone, A critical comparison of selected 1s and 2p core hole widths, *J. Electron Spectrosc. Relat. Phenom.*, 1999, **101–103**, 141–147.
45 L. Weinhardt, O. Fuchs, D. Batchelor, M. Bär, M. Blum, J. D. Denlinger, W. Yang, A. Schöll, F. Reinert, E. Umbach and C. Heske, Electron-hole correlation effects in core-level spectroscopy probed by the resonant inelastic soft x-ray scattering map of C60, *J. Chem. Phys.*, 2011, **135**, 104705.
46 F. Hennies, A. Pietzsch, M. Berglund, A. Föhlisch, T. Schmitt, V. Strocov, H. O. Karlsson, J. Andersson and J.-E. Rubensson, Resonant Inelastic Scattering Spectra of Free Molecules with Vibrational Resolution, *Phys. Rev. Lett.*, 2010, **104**, 193002.
47 N. Kovačević and A. Kokalj, Analysis of molecular electronic structure of imidazole- and benzimidazole-based inhibitors: A simple recipe for qualitative estimation of chemical hardness, *Corros. Sci.*, 2011, **53**, 909–921.
48 G. Zhang and C. B. Musgrave, Comparison of DFT Methods for Molecular Orbital Eigenvalue Calculations, *J. Phys. Chem. A*, 2007, **111**, 1554–1561.

49 E. Apen, A. P. Hitchcock and J. L. Gland, Experimental studies of the core excitation of imidazole, 4,5-dicyanoimidazole, and s-triazine, *J. Phys. Chem.*, 1993, **97**, 6859–6866.
50 M. Ekimova, W. Quevedo, Ł. Szyc, M. Iannuzzi, P. Wernet, M. Odelius and E. T. J. Nibbering, Aqueous Solvation of Ammonia and Ammonium: Probing Hydrogen Bond Motifs with FT-IR and Soft X-ray Spectroscopy, *J. Am. Chem. Soc.*, 2017, **139**, 12773–12783.
51 J. S. Uejio, C. P. Schwartz, A. M. Duffin, A. England, D. Prendergast and R. J. Saykally, Monopeptide versus Monopeptoid: Insights on Structure and Hydration of Aqueous Alanine and Sarcosine via X-ray Absorption Spectroscopy, *J. Phys. Chem. B*, 2010, **114**, 4702–4709.
52 H. Ågren, Y. Luo, F. Gelmukhanov and H. J. A. Jensen, Screening in resonant X-ray emission of molecules, *J. Electron Spectrosc. Relat. Phenom.*, 1996, **82**, 125.
53 F. Gel'mukhanov and H. Ågren, Resonant inelastic x-ray scattering with symmetry-selective excitation, *Phys. Rev. A*, 1994, **49**, 4378–4389.

Imidazole	N1	N3	C2	C4	C5
XES	0	+0.45	+0.75	+0.55	+0.57
XAS	+0.75		+0.74	+0.64	
Imidazolium					
XES	-0.70		-0.30		
XAS	-0.40		-0.20	-0.60	

Table 1: Energy shifts (in eV) used to align the calculated XES and XAS spectra with the experimental data.

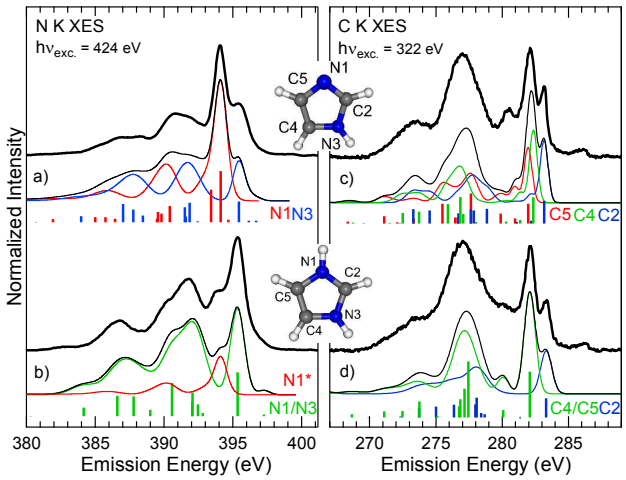

Figure 1: Non-resonant N K XES spectra of Im (a) and ImH^+ (b), and C K XES spectra of Im (c) and ImH^+ (d), shown as black thick lines. The labels of the individual atoms are given in the depicted molecular structures. Below each spectrum, calculated XES line intensities are shown as vertical bars, color-coded for the non-equivalent nitrogen and carbon atoms. The correspondingly colored lines give the calculated spectra after Gaussian broadening, and the sums of the individual contributions are depicted by black thin lines. $N1^*$ denotes the calculated spectrum for N1 in Im, and represents spectral contributions in the spectrum of Im^+ caused by nuclear dynamics.

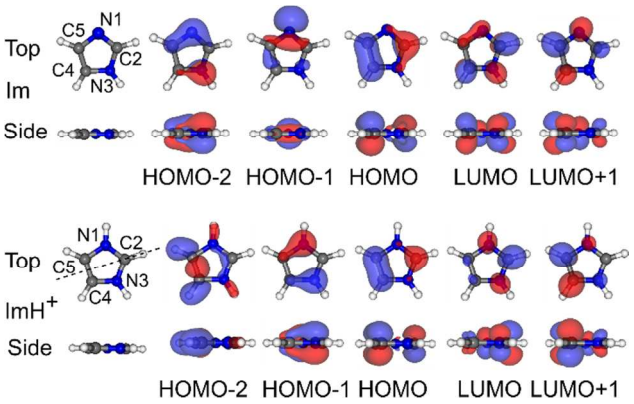

Figure 2: Calculated isodensity surfaces of the three highest occupied and two lowest unoccupied molecular orbitals of Im (top) and ImH^+ (bottom), respectively (isosurface value: $\pm 0.07 \frac{e}{a_0^3}$).

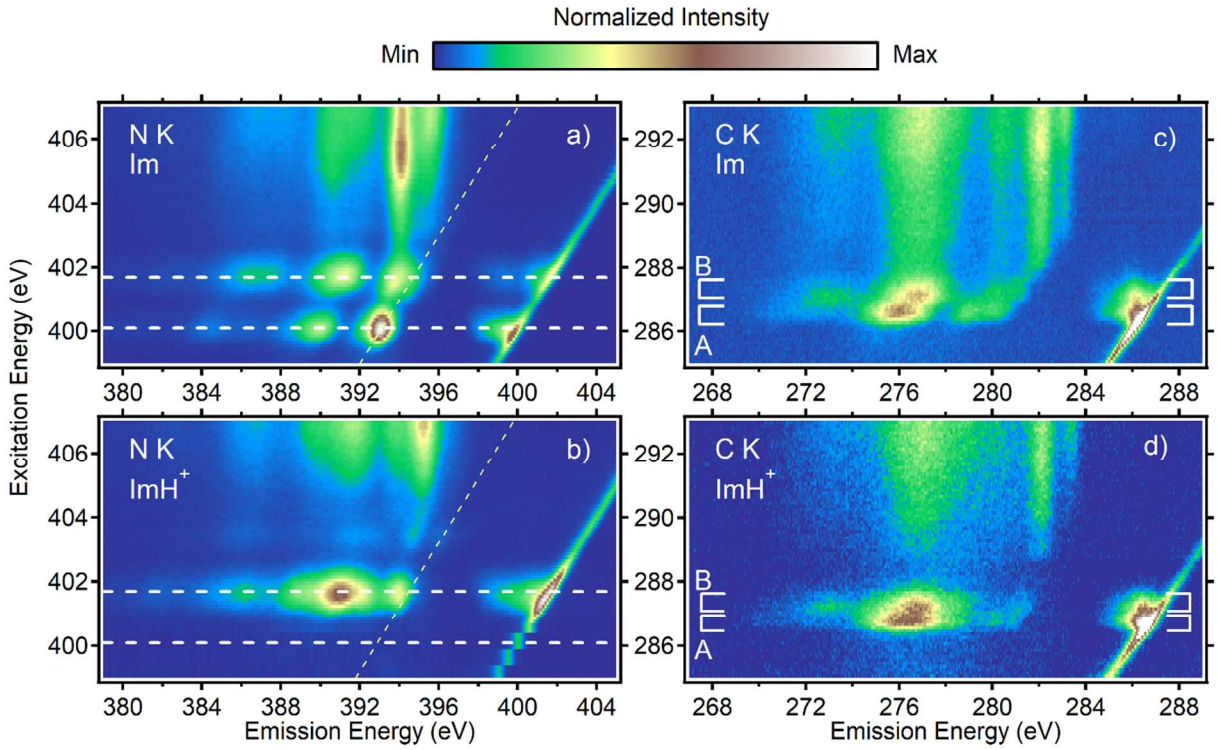

Figure 3: N K RIXS maps of Im (a) and ImH^+ (b), as well as C K RIXS maps of Im (c) and ImH^+ (d). The RIXS intensity is color-coded and displayed as a function of excitation and emission energy. Excitation energies and ranges corresponding to specific XAS resonances are marked by white dashed lines (a and b) and white brackets and labels "A" and "B" (c and d). The yellow line indicates the HOMO-2 to LUMO (Im) and HOMO-1 to LUMO transition (ImH^+).

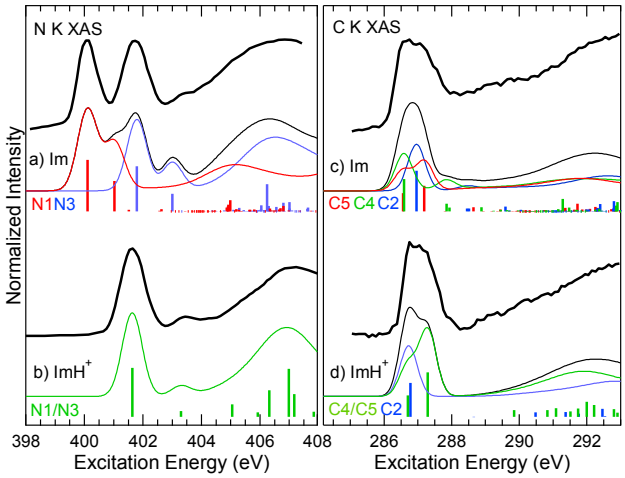

Figure 4: Black thick lines represent the partial fluorescence yield N K XAS spectra of Im (a) and ImH^+ (b), as well as C K XAS spectra of Im (c) and ImH^+ (d). The intensity was derived from the RIXS maps in Fig. 3 by integrating the entire spectator region at each excitation energy. Below each spectrum, calculated XAS line intensities are shown as vertical bars, color-coded for the non-equivalent atoms. The correspondingly colored lines give the calculated spectra after Gaussian broadening, and the sums of the individual contributions are depicted by black thin lines.

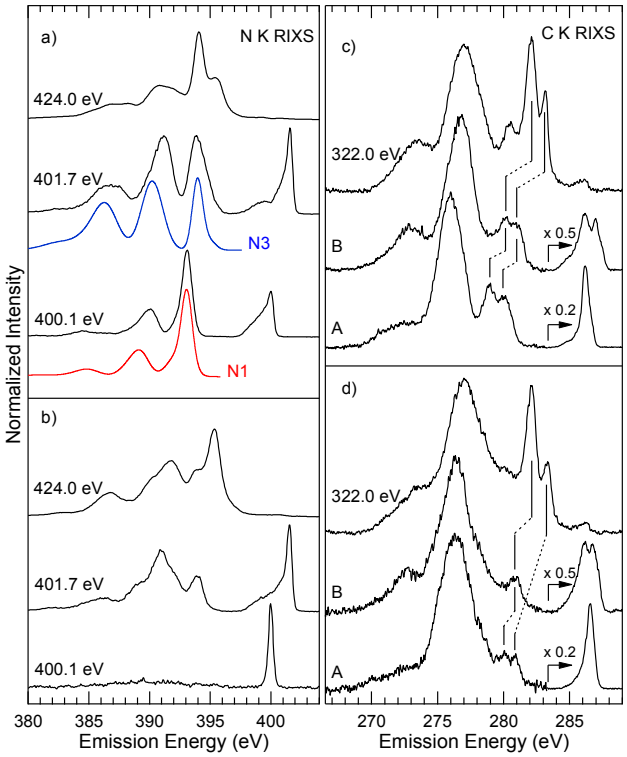

Figure 5: N K RIXS spectra of Im (a) and ImH^+ (b), as well as C K RIXS spectra of Im (c) and ImH^+ (d). The excitation energies and energy ranges ("A" and "B", defined in Figure 3) are specified next to the respective spectra. In a), calculated non-resonant spectra are given for comparison in red (N1) and blue (N3). For the C K RIXS spectra, the intensity in the participant region was scaled by the stated factors.

The electronic structure of aqueous imidazole and imidazolium solutions is studied in an atom- and site-specific fashion using x-ray spectroscopy.